AIAA-2007-0111

45th AIAA Aerospace Sciences Meeting and Exhibit 8 - 11 Jan 20067, Reno, Nevada

Shift Modes and Transient Dynamics in Low Order, Design Oriented Galerkin Models

Gilead Tadmor* and John Gonzalez†

Communication & Digital Signal Processing Center

Northeastern University, 440 Dana Research Building, Boston, MA 02115, USA

Oliver Lehmann‡ and Bernd R. Noack§

Institute of Fluid Dynamics and Technical Acoustics

Berlin University of Technology, Straße des 17. Juni, D-10623 Berlin, Germany

Marek Morzyński¶ and Witold Stankiewicz‖

Institute of Combustion Engines and Transportation

Poznań University of Technology, Ulica Piotrowo 3, 60-965 Poznań, Poland

The *shift mode* has been introduced in Ref. [1] as a critical enabler for transient representation of very low dimensional empirical Galerkin models in fluid flow systems. As introduced[1] and used in a number of flow control studies since, the shift mode is a simple representation of a missing dynamic mean-field correction, pointing from an unstable steady solution to a stable natural attractor. In this study we explore alternative local definitions of the shift mode, their interdependence and consistency. In particular, we investigate short term proper orthogonal decomposition of natural and controlled transients. In addition, the mean-field directions are estimated from short term analysis of simulations, and from the corresponding Reynolds stress equation.

I. Introduction

Very low order Galerkin models are commonly based on modes representing the dominant instability in the flow. This is the standard practice both in models using linear stability analysis eigenmodes, and in empirical models, using Karhunen-Loève modes[2–8] of the velocity field, which are similar to the eigenmodes[a]. A common deficiency of such models is their difficulty to provide reliable transient predictions, away from the linearization point or from the reference orbit from which empirical modes were extracted[10] . This deficiency is detrimental to the use of the reduced order Galerkin models in applications such as feedback control design, where transient representation capabilities and very low dimension, are both essential. A key factor is the exclusion of flow structures orthogonal to the hyperplane spanned by the low order approximation. Karhunen-Loève modes or similar eigenmodes, representing the instability, span a hyperplane providing a

*Professor, CDSP Director

†Graduate student

‡Student

§Ass. Professor

¶Professor

‖Research Fellow

[a]Indeed, as we have recently shown,[9] empirical proper orthogonal decomposition modes can, in fact, be approximated in terms of linear stability eigenmodes. We shall revisit an implication of this point later.

good approximation of the natural (or control-stabilized) attractor, but do not capture changes in the mean flow that are orthogonal to the attractor. Yet dynamic interactions between the mean flow and leading coherent structures with the mean flow is critical to the physics of the flow system, and to the stabilization of unsteady attractors[1, 11–14].

Following the basic premises of mean-field theory[11], we have introduced the *shift mode*[1, 15] as a POD model augmentation that represents the dynamics and stabilizing effect of mean field corrections and is thus a key enabler for the representation of transient dynamics. The laminar flow behind a circular cylinder is a case in point, where a mere three dimensional, Landau-type model is capable of capturing all the key dynamic properties of the transient manifold, connecting the unstable steady solution and the natural, periodic attractor. It is therefore also a key component in the development of a Galerkin model based feedback flow control toolkit[16–18]. Similar observations regarding the significance of dynamic changes in the base flow, and indeed, least order Landau (and Ginzburg-Landau) models, featuring the stabilizing effects of the interactions of flow instabilities with the base flow were made by other authors, in a variety of contexts and configurations[11–14, 19, 20].

As will be established, mean field corrections along naturally and continuously actuated transients are locally asymptotically dominated by a single vector field. That single direction represents the flow structure that is responsible for the dynamic energy exchange and balancing between the dominant instability and the base flow, at the selected operating condition. Thus, that direction will dominate, e.g., the slow, non-oscillatory base flow changes in the velocity field, as transients approach an investigated natural or feedback controlled attractor, or depart from an unstable operating point. Natural, local definitions of the shift mode therefore include the dominant POD mode(s) of low-pass filtered empirical transient data, and from Reynolds stress based analysis. Such definitions can be associated with selected attractors, unstable points, or simply the means of periods, along a transient. The definition of the shift mode in[1] was based on a search for the least order model that includes the missing phase space direction, which is the velocity field pointing from the steady solution, $\mathbf{u}_s$, to the mean of the natural attractor, $\mathbf{u}_0$. That is, the shift mode was defined as the normalized difference: $\mathbf{u}_\triangle \propto \mathbf{u}_0 - \mathbf{u}_s$. The purpose of the current study is to explore in detail the local nature of the shift mode, and the consistency of the several alternative, plausible definitions, mentioned above. The paper uses the laminar flow behind the circular cylinder as a benchmark.

II. The Cylinder Wake Benchmark and Reference Trajectories

The Laminar Wake Flow Behind the 2D Cylinder

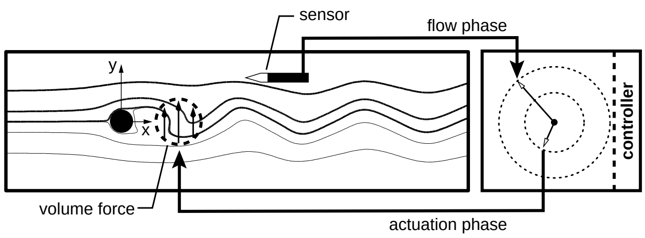

Figure 1. A sketch of the actuated cylinder wake. The cylinder is represented by the black disk. The location and orientation of a postulated volume-force actuator are indicated by the downstream circle and arrows. Streamlines represent the natural flow. The figure includes a hot-wire anemometer at a typical experimental position. This sensor has been used in an observer-based, closed-loop control,[15, 18] to determine the actuation phase and amplitude.

The laminar, two dimensional flow in the circular cylinder wake becomes unstable at $Re \approx 47$, and is considered here at $Re = 100$. The natural flow converges to a periodic attractor, dominated by von Kármaán vortex shedding. The flow field is then strongly dominated by the first temporal harmonic at the shedding frequency. Indeed, the dominant POD mode pair resolves some 95% of the attractor perturbation kinetic energy[10]. Similarly, the early transient, initiated by a small perturbation of the unstable, steady solution, is dominated by the two eigenmodes, associated with the instability, and, in fact, perturbations from short time averages, at any point along the natural transient, are similarly dominated by a single pair of coherent flow structures. A technically facilitating aspect for the analysis in this paper is the spatial symmetry of this benchmark. It implies that the dominant modes representing the instability are distinguished by anti-symmetry with respect to the horizontal midline, as are the modes representing subsequent odd harmonic of the main shedding frequency.

While direct manifestations of the instability, including the modes mentioned right above, are at the center of attention in most discussions of the cylinder (and similar bluff body) wake flows, our focus here is rather on the indirect manifestation, in terms of the non-oscillatory, slowly varying aspect of the flow. Indeed, our preliminary processing effort is dedicated to extract the non-oscillatory component from the flow, and exclude the oscillatory part, as explained in Section III. The anti-symmetry property mentioned above comes handy, in this respect (but is not essential, as detailed in[21]). In particular all the figures shown in this paper are dedicated to the non oscillatory component of the flow. Depictions of the oscillatory flow structures abound and can be easily found in the voluminous wake flow literature, including our own[1].

Figure 1 provides a schematic picture of the cylinder wake benchmark, where stream lines represent the natural flow over the computational domain of $\Omega = \{\mathbf{x} = (x, y) : x \in [-5, 15], y \in [-5, 5]\}$ (non-dimensionalizing distance with respect to the cylinder diameter). The cylinder is represented by the black disk. The empirical data used in this paper was produce by direct numerical simulations (DNS) of the incompressible Navier-Stokes equations, using an 8712 nodes, symmetric grid over the specified domain, and a first order interpolation of the integral.

Figure 1 also includes a postulated vertical volume-force actuator, supported over a downstream disk, and a hot-wire anemometer - a fluid velocity sensor - representing flow sensing, as previously discussed in[15,18]. A common flow control objective, in this configuration, is therefore to suppress this instability which causes mechanical vibrations and increased drag[22–25]. In the context of that design objective, modeling efforts are focused on the dynamic range of transients between the desirable steady solution, and the natural attractor.

Reference Trajectories

One of the two references used in this note is the natural transient, from a small perturbation of the unstable, steady solution of the Navier-Stokes equations to the natural attractor. In what follows we shall parameterize the instantaneous operating point in terms of the kinetic energy, $\mathcal{K}$, of the flow field perturbation from its short time average (more details are provided Section III). The left plot in Figure 2 depicts the time trajectory of $\mathcal{K}$, in that simulation.

Actuation is employed here merely as a tool to generate the second of the two reference trajectories used in this note. We therefore opt for the simplest control, physically motivated control policy, by which actuation is applied as a dissipative deceleration force: With a commanded volume force amplitude of $b(t)$, the *energy extraction rate* $-b(t) \int_{\Omega} dV \mathbf{g}(\mathbf{x}) \cdot \mathbf{u}(\mathbf{x}, t) = -b(t) (\mathbf{g}, \mathbf{u}(\cdot, t))$, where $\mathbf{g}$ is the volume force field and $\mathbf{u}(\cdot, t)$ is the instantaneous velocity field. $G(t) = -k (\mathbf{g}, \mathbf{u}(\cdot, t))$ therefore creates a dissipative force, and the gain $k > 0$ determines the dissipation rate. The gain value k was ramped up, and then down, in a manner, that the decay of the perturbation kinetic energy (TKE) is (approximately) linear in time. Specifically, k was stepped in 17 consecutive segments, in each of which it was ramped linearly. The controlled trajectory started at the natural attractor, reached a nearly fully attenuated flow, and then returned to the natural attractor. Figure 2 summarizes key facts regarding these two, main reference trajectories used in this note.

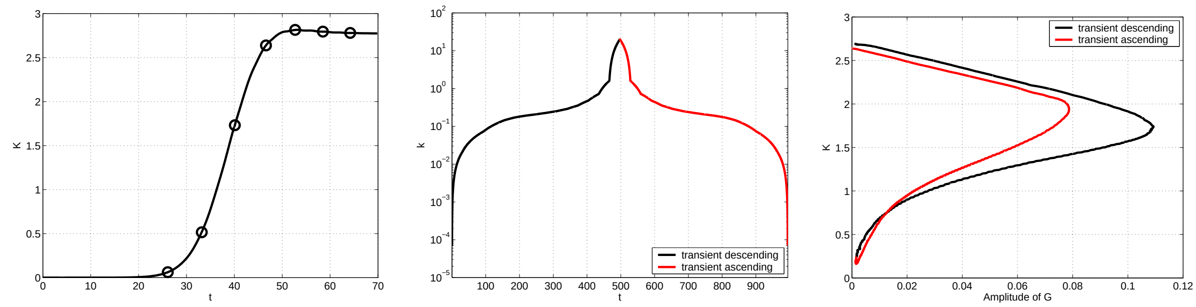

Figure 2. Aspects of the two main reference simulations used in this discussion. Left: Time trajectory of the perturbation energy of the natural transient from the steady solution to the attractor. The circle indicate the time and energy levels at the center of 7 periods used to obtain local shift modes. Middle: Time trajectory of the dissipative feedback gain, $k(t)$, in the forced trajectory from the natural attractor to steady flow and back. Right: The perturbation energy as a function of the corresponding amplitudes of the applied feedback force $G(t) = -k(t) (\mathbf{g}, \mathbf{u}(\cdot, t))$. Black: the descending trajectory, requiring higher actuation force, and Red: the ascending trajectory, requiring a lower force, as the flow is allowed to gradually return to the natural attractor.

III. Preliminary Processing: Extraction of Mean Flow References

Our goal is to extract from the reference trajectory the slowly varying, non-oscillatory component of the flow. This issue is discussed in[21], in a more general frequency separation context, as well as for a more challenging asymmetric configuration. Here we can exploit the afore mentioned spatial symmetry with respect to horizontal midline: At steady state, odd temporal frequencies are represented by the anti-symmetric component of the flow field, whereas even temporal frequencies – in particular, the mean field – are included in the symmetric component. This remains a good approximation during moderate transients. The symmetric part of perturbations from a fixed base flow is dominated by slow changes in the mean field and by the second temporal harmonic. Extraction of the time varying base flow therefore followed these next two steps:

(a) Exclude the first and higher odd temporal harmonics of the flow field. This is done by extraction of the instantaneous spatially symmetric component, discarding the anti-symmetric part.

(b) Exclude the second and higher even temporal harmonics of the flow field. This require temporal filtering: at the time t, one window-average the flow field

$$\mathbf{u}_b(\mathbf{x},t) \doteq \int_{t-0.5T}^{t+0.5T} \mathbf{u}(\mathbf{x},\tau)\, d\tau$$

where the window length τ is an integer multiple of half a period.

Step (b) is challenging due to the fact that the shedding period vary considerably over the range of the operating conditions we are interested in. That is, the period $T(t)$ is time varying. There are various heuristics to determine a robust concept of an instantaneous period in the current framework. Following is a description of the procedure we used here and in other, similar situations. Let $\mathbf{u}_i$, $i = 1, 2$, be the dominant POD mode pair for the natural attractor, representing the dominant vortex shedding harmonic, and let $a_i(t)$ be the respective Fourier coefficients along the reference trajectory of interest. These two coefficients can be written in the form

$$a_1(t) = A_1(t) + R_1(t)\cos(\phi(t)) \qquad a_2(t) = A_2(t) + R_1(t)\sin(\phi(t))$$

where $A_1(t)$, $A_2(t)$, $R_1(t)$ and $\omega(t) \doteq \frac{d}{dt}\phi(t)$ are slowly varying relative to the instantaneous period $T(t) \doteq 2\pi/\omega(t)$, and $A_i(t)$ are nearly zero. The latter, "*dc*" components can be safely estimated by sufficiently large / multiple periods window averages, even when the used window length is inaccurate as a period multiple. Having removed these components, the phase $\phi(t)$ is estimated as $\tan^{-1}$ of the two coefficients. The instantaneous frequency is then estimated as the tangent of a straight line approximation of the graph of $\phi(t)$ over a moving window of about one period. (Again, the result is insensitive to the window length.) This method is reminiscent of the common practice for representation of alternative-currents ("*ac*") in power engineering, as the sum of instantaneous harmonic coefficients termed the *direct* and *quadrature phasors*. It is noted that analysis of the base flow / mean-field obtained this way that still reveals traces of the second harmonic, showing that even though the method described here is relatively robust, the harmonic separation of transient trajectories is an intrinsically difficult task.

From this point on, mentioning of the the *reference base flow trajectory* should be interpreted as the slowly varying, non-oscillatory component of the reference trajectory.

IV. Local Shift Mode Extraction

We present and later compare several methods to estimate the velocity field orientations of local mean-field corrections. Those will include the following:

(i) The entire transient reference base flow will be approximated by its dominant POD modes. The first, most dominant of those modes is one candidate for a *global shift mode*. This analysis was applied to the natural transient.

(ii) The POD approximation, in Step (i), provide a low dimensional approximation of base flow variations

$$\mathbf{u}_b(\mathbf{x},t) \approx \mathbf{u}_0(\mathbf{x}) + \sum_i a_{b,i}(t)\mathbf{u}_i(\mathbf{x})$$

Using this approximation, the orientations of the local mean-field correction is estimated by a linear combination of the (low-pass filtered) time derivative of the Fourier coefficients:

$$\mathbf{u}^t_\Delta(\mathbf{x}) \doteq \sum_i \frac{d}{dt} a_{b,i}(t)\mathbf{u}_i(\mathbf{x})$$

(iii) Using the instantaneous period approximation, as described in Section III, the local shift mode, $\mathbf{u}^t_\Delta(\mathbf{x})$, is estimated as the dominant POD mode of the base flow transient over a single period, centered at the time t. Conceptually, the relation of this estimate to the local estimate by method (ii), above, is analogous to the relation between finite differences and actual derivatives. This approach was applied to both the natural and the forced transients.

(v) The velocity field $\mathbf{u}_b(\mathbf{x},t)$ is the mean of the period, centered at the time t. We ran short simulations, initiated at these points and extracted the dominant POD modes of the base flow components, of these short simulations. The substitution of the original transient trajectory by the proximity of a single point makes the approach underlying these computations closer in spirit to what would be obtained by linear stability analysis.

(iv) Using $\mathbf{u}_b(\mathbf{x},t)$ once again as a point of reference, the dominant component of the linearize Reynolds stress is an *a priori* analytic estimate of the direction of mean field change.

This range covers a variety of empirical and analytic approaches. In what follows we shall provide details on the specifics of each of the computations, compare their results and conclude with a discussion of the consistency of the local and global shift mode concepts.

IV.A. Global Base Flow Analysis of the Natural Base Flow Transient

Figure 3 depicts the POD eigenvalues, normalized with respect to the largest one, the mean field and the first five leading POD modes of the entire natural base flow transient. As seen, the first five eigenmodes decay at a roughly fixed exponential rate. The velocity fields of subsequent eigenmodes (not shown) have the the typical structure of second harmonic POD modes, and are therefore due to (minor) numerical contamination of the extracted base flow reference. Indeed the first mode, alone, provides an average resolution of some 94.5% of the perturbation along this transient, and the first three modes provide a near perfect reconstruction, with an average of 99% the entire transient. These numbers, however, should be taken in proper perspective, since time averaging does not provide equal spacing, e.g., with respect to perturbation amplitude. As we shall see in Section V, a single mode will provide a somewhat less impressive resolution of local shift modes, but three modes are certainly ample.

The following two observations are significant in their own right:
A single mode provides a good, albeit imperfect approximation of the entire base flow trajectory. This mode is nearly identical to the global mean field correction, provided by $\mathbf{u}_\Delta \propto \mathbf{u}_0 - \mathbf{u}_s$, an observation that lends additional support to the empirical mean-field model proposed in[1] and used for model-based feedback control of wake flows[15, 16, 18–20] .

Base flow variations are slow and confined to a low dimensional space. We have so far shown an indication of this statement for the natural transient. Subsequent analysis of the similarity between local shift modes will substantiate this claim. Again this observation is essential for the validity for the basic mean-field theory tenets regarding the role role of such structures in the transient and attractor behavior of unstable flows.

We have extracted the local *incremental local shift mode* from the trajectories of the dominant three Fourier coefficients, as explained in option (ii), at the beginning of Section IV. Depictions of three such modes are shown in Figure 4. The sensitivity of this method is reflected by the presence of typical second harmonic substructures (the smaller symmetric close orbits).

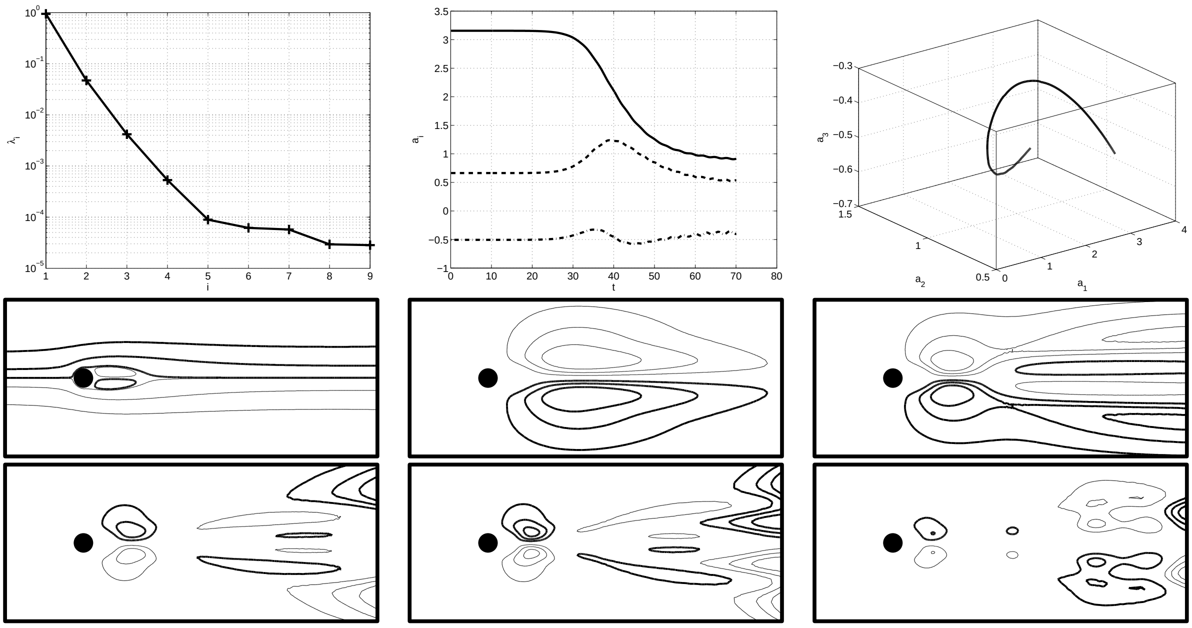

Figure 3. **POD analysis of the entire natural base flow transient. Top, left: POD Eigenvalues. Top, middle and right: The Fourier coefficients of a three-modes approximation of the natural base flow transient. Following two rows: The mean field and the dominant first five POD modes, visualized by streamlines, shown by that order, from left to right and from top to bottom.**

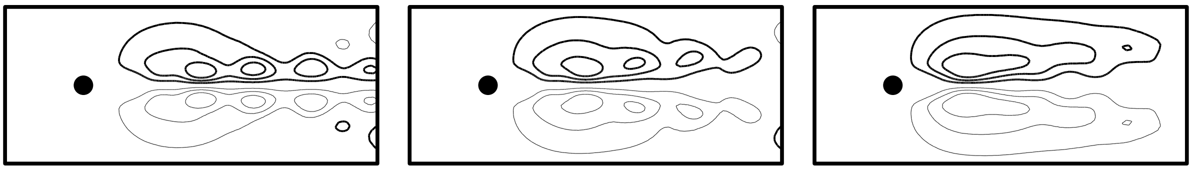

Figure 4. **Examples of three incremental local shift modes obtained as time derivatives of the three-modes POD approximation of the entire natural base flow transients. The modes are visualized by streamlines.**

IV.B. Shift Modes of natural Transient Periods

We have analyzed seven periods of the natural attractor. These periods are parameterized by their respective levels of perturbation energy, as defined earlier. The values energy levels of 0.09596, 0.69154, 1.97177, 2.68725, 2.78488, 2.78635 and 2.79097, can be put in perspective, against the global plot of the perturbation energy in the natural attractor. The top left and middle plots in Figure 5 provide two depictions of the dominant POD eigenvalues for these seven operating points. The left figure is in the standard form of a logarithmic plot of the eigenvalue amplitudes (normalized with respect to the first eigenvalue, at each operating point), as a function of the eigenvalue number. This plot reveals the fast decay of the eigenvalues and, indeed, the fact that each of the periods is dominated by a single dominant mode. Invariably, the second POD eigenmodes, in each of the periods, was dominated by second harmonic structures, strengthening the statement regarding the local single shift mode dominance.

The middle figure of the top row shows again the normalized values of the four dominant eigenvalues, now as a function of the operating conditions, making it easier to compare the decay rates. The dominant eigenmode of each of the seven operating conditions, are visualized by streamlines, in the remaining seven plots, in Figure 5. These plots reveal both the overall similarity and the continuous deformation of the local shift modes, as the operating condition changes.

IV.C. Shift Modes of Actuated Transient Periods

Similar to what was described in the preceding section, we have analyzed periods of the actuated trajectory. Here we used 155 overlapping periods, covering the entire transient from the natural attractor to a fully attenuated flow and back. The top left plot in Figure 6 is a counterpart of the middle top plot in Figure 5, comparing the (individually normalized) dominant POD eigenvalues as a function of the period index.

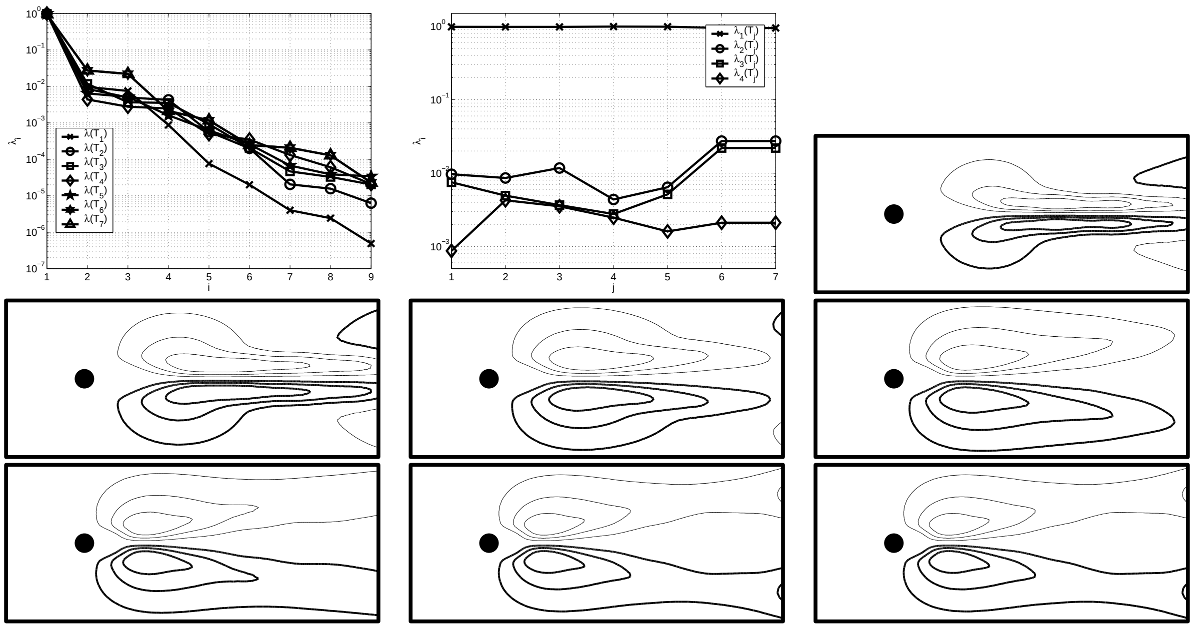

Figure 5. POD analysis of seven periods of the natural base flow transient. Top, left: normalized POD Eigenvalues at the seven periods, plotted as a function of the eigenvalue number. Top, middle: The dominant four eigenvalues, now plotted as a function of the period number. From there on, from left to right and top to bottom, the dominant POD mode of each of the periods, visualized by streamlines.

Again, the dominance of a single POD mode in each period is apparent, both from the POD eigenvalues and from the fact that, invariably, the second and third eigenmodes are actually second harmonic modes. Figure 6 also presents the plots of eight eigenmodes of eight periods, representing the entire range of the forced transient.

IV.D. Shift Modes of Short Transients From Period Means

Here, short transient trajectories we obtained from simulations initiated at the means of the seven periods of the natural base flow transient, that were discussed in Section sIV.B. For these short simulations, the dominance of the symmetrized flow by a single mode needs no argument, and the computation is simply a simulation-based approximation of the symmetric part of the vector-field, at the chosen points. Figure 7 provides plots of these seven modes, which are counterparts of the modes presented in Figure 5.

IV.E. Shift Modes Based on The Reynolds Stress at Period Means

The Reynolds Stress provides the forces imposed on the mean flow by turbulent fluctuations. It is therefore a natural estimate for the local direction of mean field corrections. POD analysis of individual periods yields the dominant mode-pair for the oscillatory component of the flow and the Reynolds stress can thus be estimated. Our last estimate of the local Shift modes is based on this approach. It was applied at the same seven operating points as in Sections IV.B and IV.D. The modes are depicted in Figure 8.

V. Comparison of Local Shift Modes

The first comparison, in Figure 9, concerns the agreement between the POD approximation of the entire natural base flow transient and the local shift modes, obtained by POD approximation of individual periods, of the same transient. The best resolution by a single long term modes is of the local shift mode obtained from period No. 4, near the mid-transient. The worst single mode resolution deteriorates to about 65%, demonstrating that the mean-field correction is, in and of itself, a dynamic entity. At the same time, the fact that the resolution reaches 98%, when 3 long term modes are employed, substantiates the earlier claim regarding the limited variation in the mean-field correction.

The comparison of the many estimates of local shift modes, by different methods and at multiple operating

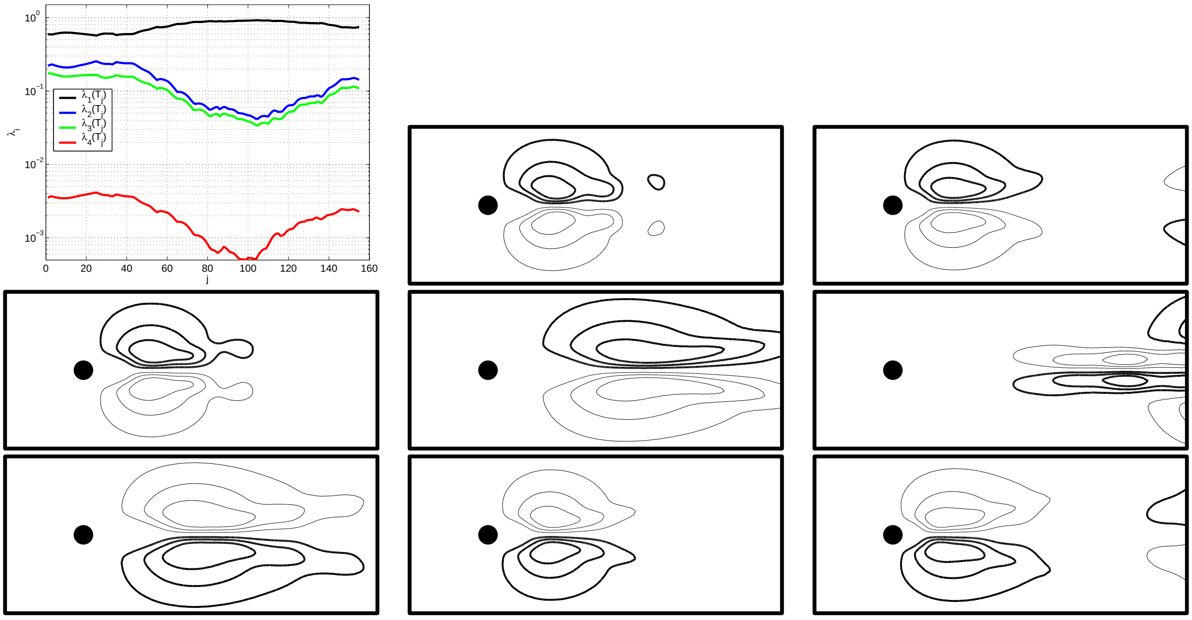

Figure 6. POD analysis of 155 periods of the forced base flow transient. Top, left: normalized POD Eigenvalues, plotted as a function of the period number. From there on, from left to right and top to bottom, the dominant POD mode at eight periods, visualize by streamlines.

conditions, is quantified by the absolute values of the respective inner products. In Figures 10 and 11 we present these results by color visualization of the (absolute values) of the entries of the respective correlation matrices. Figure 10 visualizes the correlation of shift modes obtained from POD of periods of the ascending and descending components of the forced transient (left plot), and of the forced transient with short term modes from the natural transient (middle and right plots). While the manifestation of numerical issues is manifest in the first plot, the main diagonal dominance, with correlation value of near unity, validate the consistency of the definition. At the same time, lower values, away from the main diagonal, demonstrate the operating point dependence of the local shift mode. The fact that the maximum correlation between the forced and natural transients, in the middle and right plots, is not achieved precisely on the main diagonal is due the the effect of the large volume force on the near wake mean flow. Nonetheless, the strong diagonal-like skeletal dominance of the plots demonstrates a consistent dependence on the operating condition.

The second set of correlation matrices, in Figure 11, compares the local shift modes obtained from periods of the natural base flow transient, the local shift modes extracted from short transients, initiated at the respective means of the same periods, and finally, the corresponding Reynolds stress estimates. An interesting observation is that the highest correlation of a local shift mode, obtained from a period of the natural base flow transient at a certain operating point, with either the local shift modes extracted from a short transient, initiated at period means, and from the Reynolds stress estimates is when the latter two are computed at an operating point of a higher perturbation energy. This observation is in agreement with our observation in,[9] concerning modes interpolation: Roughly stated, the observation in that paper implies that the POD modes of the natural attractor can be best matched by linear stability eigenmodes that are obtained at a controlled attractor of a higher perturbation energy. The joint observation is therefore that the flow orientation near an attractor, or cycle mean is similar to its transient behavior at a higher perturbation level.

Finally, we selected a single perturbation level, at $\mathcal{K} = 2$, and provide a detailed comparison of all the six local shift modes, obtained at that level. Figure 12 provides visualizations of these six modes, and the table, included at its caption, provides the (absolute values) of the mutual correlations between these modes. The table illustrates the fact we have already noted, that the best correlation is not between the different modes at the same level of perturbation, making this aspect of the shift mode definition a sensitive to both the method of computation, and the nature of the transient. For example, from Figure 11 we expect the shift modes obtained from POD modes of periods, both natural and forced, should correlate well with Reynolds stress shift modes obtained at a higher perturbation level.

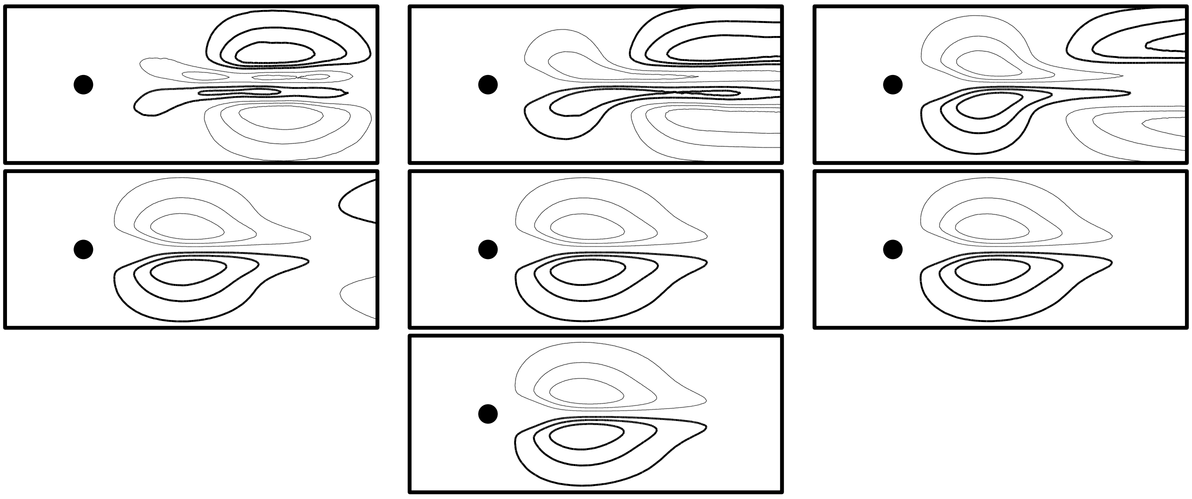

Figure 7. From left to right, from top to bottom, local shift modes extracted as the dominated modes of short term simulations, initiated at the center of periods of the natural transient. The Modes are visualized by streamlines.

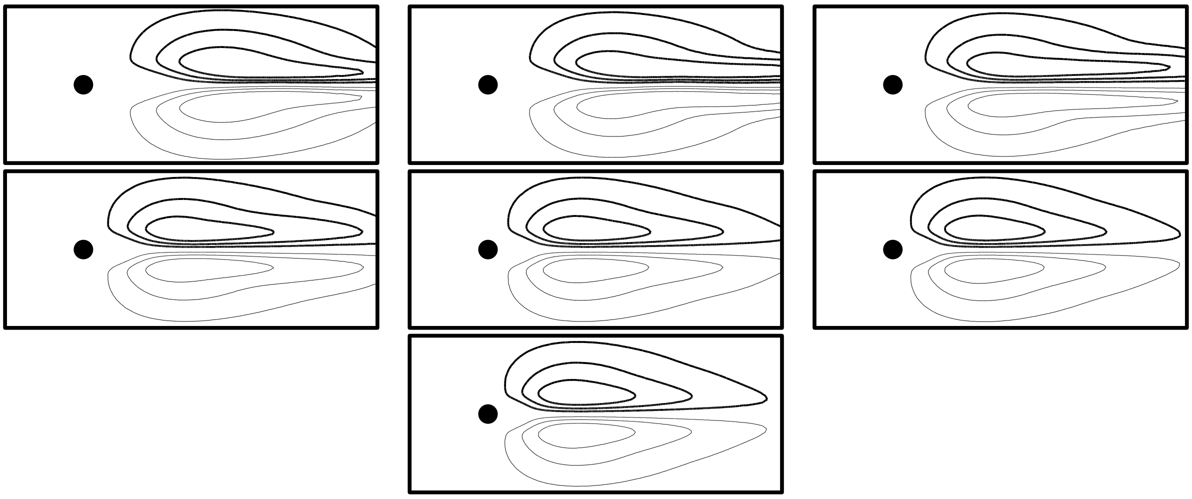

Figure 8. From left to right, from top to bottom, local shift modes extracted using the Reynolds stress estimate of the orientation of the local mean-field force, at the same operating points as in Figures 5 and 7.

Acknowledgments

We acknowledge funding from the Deutsche Forschungsgemeinschaft (DFG) under grants No. 258/1-1 and No. 258/2-3 and via the Collaborative Research Center (Sfb 557) "Control of complex turbulent shear flows" at the Berlin University of Technology, the U.S. National Science Foundation (NSF) under grants No. 0524070, 0410246 and 0230489, and US Air Force Office of Scientific Research (AFOSR) under grants FA9550-0610373 and FA9550-0510399. The authors acknowledge stimulating discussions with Laurent Cordier, Rudibert King, Michael Schlegel, Mark Pastoor, Mark Luchtenburg, Jon Scouten and Tino Weinkauf. We are grateful for outstanding hardware and software support by Lars Oergel and Martin Franke at TU Berlin.

References

[1]B.R. Noack, K. Afanasiev, M. Morzyński, G. Tadmor, and F. Thiele. A hierarchy of low-dimensional models for the transient and post-transient cylinder wake. *J. Fluid Mech.*, 497:335–363, 2003.

[2]K. Karhunen. Zur spektralen Theorie stochastischer Prozesse. *Ann. Acad. Sci. Fennicae, Ser. A1, Math. Phys.*, 37, 1946.

[3]M. M. Loève. *Probability Theory.* VanNostrand, 1955.

[4]E. N. Lorenz. Empirical orthogonal functions and statistical weather prediction. Technical report, MIT, Department of Meteorology, 1956. Statistical Forecasting Project.

[5]V.R Algazi and D.J. Sakrison. On the optimality of the Karhunen-Loève expansion. *IEEE Trans. Inform. Theory,*

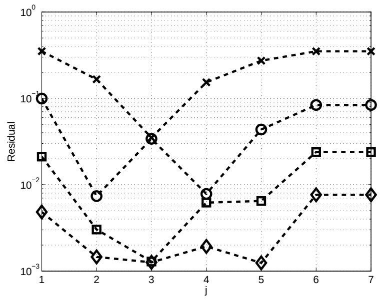

Figure 9. The resolution of the reproduction of the local shift modes, obtained as dominant POD modes of the seven periods of the natural transient, in terms of the dominant global POD modes of the entire natural transient. The plots shows the relative residual amplitude when the reconstruction employs a single, two, three and four global POD modes.

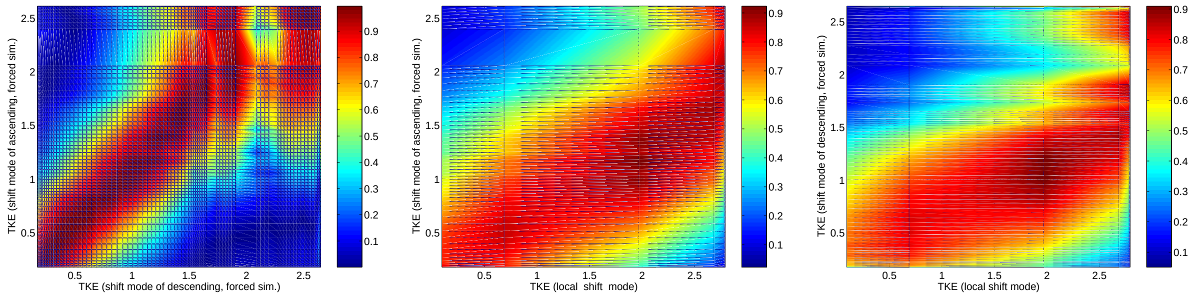

Figure 10. Correlations of shift modes obtained from POD of periods. Left: comparison of the ascending and descending components of the forced transient. Middle: comparison of the ascending component of the forced transient with short term modes from the natural transient. Right: comparison of the descending component of the forced transient with short term modes from the natural transient. The coordinate axes show the TKE of the operating conditions where the shift modes were obtained. The color codes the absolute values of the inner product.

15:319–321, 1969.

[6]L. Sirovich. Turbulence and the dynamics of coherent structures, Parts I–III. *Quart. Appl. Math.*, XLV:561–590, 1987.

[7]P. Holmes, J.L. Lumley, and G. Berkooz. *Turbulence, Coherent Structures, Dynamical Systems and Symmetry.* Cambridge University Press, Cambridge, 1998.

[8]T. R. Smith, J. Moehlis, and P. Holmes. Low-dimensional modelling of turbulence using the Proper Orthogonal Decomposition: A tutorial. *Nonlinear Dynamics*, 41:275 – 307, 2005.

[9]M. Morzyński, W. Stankiewicz, B. R. Noack, R. King, F. Thiele, and G. Tadmor. Continuous mode interpolation for control-oriented models of fluid flow. In *International Conference on Active Flow Control, Berlin, Germany*, September 28-30, 2006. Invited.

[10]A.E. Deane, I.G. Kevrekidis, G.E. Karniadakis, and S.A. Orszag. Low-dimensional models for complex geometry flows: Application to grooved channels and circular cylinders. *Phys. Fluids A*, 3(10):2337–2354, 1991.

[11]J.T. Stuart. On the non-linear mechanics of hydrodynamic stability. *J. Fluid Mech.*, 4:1–21, 1958.

[12]J.T. Stuart. Nonlinear stability theory. *Ann. Rev. Fluid Mech.*, 3:347–370, 1971.

[13]J. Dušek, P. Le Gal, and P. Fraunie. A numerical and theoretical study of the first Hopf bifurcation in a cylinder wake. *J. Fluid Mech.*, 264:59–80, 1994.

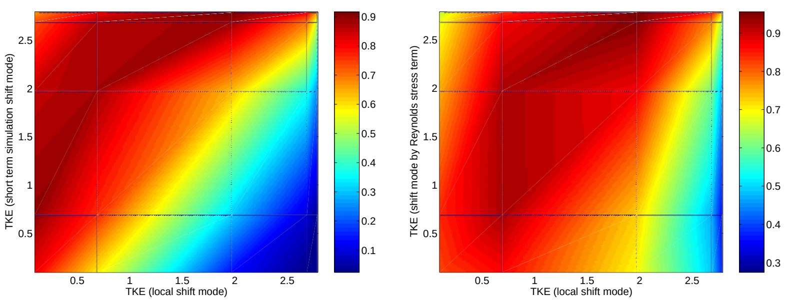

Figure 11. Left: Correlations of shift modes obtained from POD of periods of the natural base flow transient with those obtained from short transients, initiated at the corresponding period mean. Right: Correlations of shift modes obtained from POD of periods of the natural base flow transient with those obtained from the corresponding Reynolds stress estimates. Correlations are visualized as in figure 10

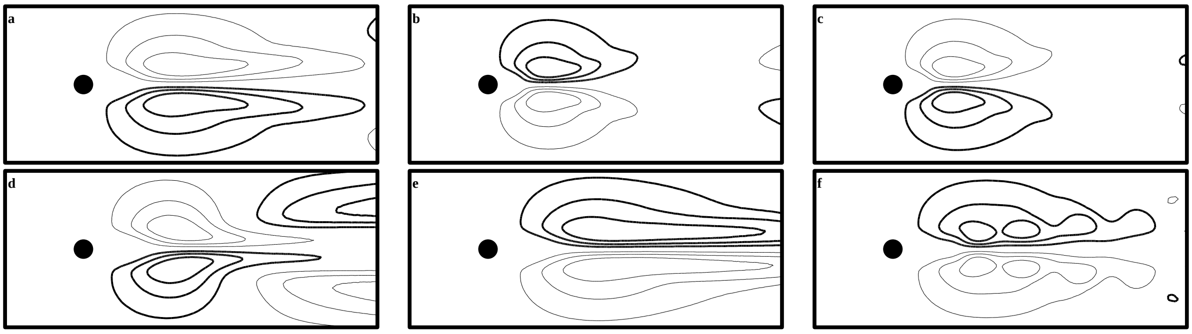

Figure 12. Local shift modes at the perturbation energy level of $\mathcal{K} = 2$: (a) POD of the period of the natural base flow transient. (b) POD of the period of the forced descending trajectory. (c) POD of the period of the forced ascending trajectory. (d) Short time transient from the period mean. (e) Shift mode obtained from the Reynolds stress estimate. (f) The instantaneous increment, obtained as a filtered time derivative of the global POD approximation of the natural transient. The table below provides the absolute values of the correlations between these modes.

	a	b	c	d	e	f
a	1.0000000	0.5685118	0.5980235	0.6297513	0.8715552	0.9330597
b	0.5685118	1.0000000	0.9919767	0.3885063	0.2691115	0.5371986
c	0.5980235	0.9919767	1.0000000	0.3838959	0.3121275	0.5562770
d	0.6297513	0.3885063	0.3838959	1.0000000	0.7007303	0.5872672
e	0.8715552	0.2691115	0.3121275	0.7007303	1.0000000	0.8090683
f	0.9330597	0.5371986	0.5562770	0.5872672	0.8090683	1.0000000

[14]BJA Zielinska, S GoujonDurand, J Dusek, and J.E. Wesfreid. Strongly nonlinear effect in unstable wakes. *Physical Rev. Letters*, 79:3893 – 3896, 1997.

[15]J. Gerhard, M. Pastoor, R. King, B.R. Noack, A. Dillmann, M. Morzyński, and G. Tadmor. Model-based control of vortex shedding using low-dimensional Galerkin models. In *33rd AIAA Fluids Conference and Exhibit*, Orlando, Florida, U.S.A., June 23–26, 2003, 2003. Paper 2003-4262.

[16]G. Tadmor, B.R. Noack, M. Morzyński, and S. Siegel. Low-dimensional models for feedback flow control. Part II: Controller design and dynamic estimation. In *2nd AIAA Flow Control Conference*, Portland, Oregon, U.S.A., June 28 – July 1, 2004. AIAA Paper 2004-2409 (invited contribution).

[17]B.R. Noack, G. Tadmor, and M. Morzyński. Low-dimensional models for feedback flow control. Part I: Empirical Galerkin models. In *2nd AIAA Flow Control Conference*, Portland, Oregon, U.S.A., June 28 – July 1, 2004. AIAA Paper 2004-2408 (invited contribution).

[18]O. Lehmann, M. Luchtenburg, B.R. Noack, R. King, M. Morzynski, and G. Tadmor. Wake stabilization using POD Galerkin models with interpolated modes. MoA15.2 In *44th IEEE Conference on Decision and Control and European Control Conference ECC, Seville, Spain*, 12.-15. December 2005.

[19]S. Siegel, K. Cohen, and T. McLaughlin. Feedback control of a circular cylinder wake in experiment and simulation. In *33rd AIAA Fluids Conference and Exhibit*, Orlando, Florida, U.S.A., June 23–26, 2003, 2003. Paper No 2003-3571.

[20]S. Siegel, K. Cohen, and T. McLaughlin. Experimental variable gain feedback control of a circular cylinder wake. In *24th AIAA Aerodynamic Measurement Technology and Ground Testing Conference*, Portland, Oregon, U.S.A., 28.6.–1.7.2004, 2004. Paper 2004-2611.

[21]G. Tadmor, M. D. Centuori, B. R. Noack, and M. Morzynski. A low order Galerkin design model for feedback flow stabilization over a 2-D airfoil. In *45th AIAA Aerospace Sciences Meeting and Exhibit*, 8 - 11 January, 2007. Paper AIAA 2007-1313.

[22]M. F. Unal and D. Rockwell. On the vortex formation from a cylinder; Part 2. Control by a splitter-plate interference. *J. Fluid Mechanics*, 190:513–529, 1987.

[23]P. J. Strykowski and K. R. Sreenivasan. On the formation and suppression of vortex shedding at low Reynolds numbers. *J. Fluid Mechanics*, 218, 1990.

[24]E. Detemple-Laake and H. Eckelmann. Phenomenology of Kármán vortex streets in oscillatory flow. *Exps. Fluids*, 7:217–227, 1989.

[25]K. Roussopoulos. Feedback control of vortex shedding at low Reynolds numbers. *J. Fluid Mechanics*, 248:267–296, 1993.